Photogearing – A Concept for Translation of Precise Motions at the Nanoscale

Aaron Gerwien,[§] *Frederik Gnannt,*[†] *Peter Mayer,*[§] *Henry Dube*[†]*

[§] Ludwig-Maximilians Universität München, Department of Chemistry and Center for Integrated Protein Science CIPSM, Butenandtstr. 5–13, 81377 Munich, Germany

[†] Friedrich-Alexander Universität Erlangen-Nürnberg, Department of Chemistry and Pharmacy, Nikolaus-Fiebiger-Str. 10, 91058 Erlangen, Germany

Abstract

Molecular machines offer the prospect of achieving highest precision for the control of dynamic processes at smallest scales. They are constructed from the bottom up and presently a growing number of building blocks such as molecular switches, rotors, and motors are available for exquisite control over local motions. The current challenge now is integrating and transmitting these motions to harness the true potential of functional nano-machinery. Molecular gearing systems allow the integration of multiple motions in a correlated fashion, to translate motions from one locality to another and to change their speed and direction. However, currently no powerful concepts exist to implement active driving of gearing motions at the molecular scale. Herein, we present a light-fueled molecular gearing system and evidence its superiority over passive thermally activated gearing. Translation of a 180° rotation into a 120° rotation is achieved while at the same time the direction of the rotation axis is shifted by 120°. Within such photogearing process, precise motions at the nanoscale can be shifted in direction and decelerated similar to macroscopic bevel-gear operations in an energy consuming way – a necessary prerequisite to employ gearing as an active component in future integrated nanomachinery.

Introduction

Control of molecular motions represents the basis for virtually all application driven chemistry fields but especially for building molecular machines and functional nanotechnology from the bottom up.(*1-5*) Steep progress has been made in this endeavor with the developments of

molecular switches,(*6*) rotors,(*7, 8*) walkers,(*9, 10*) gyroscopes, or pumps,(*11, 12*) and especially motors.(*13-27*) However, at present a standing challenge for further advances is the integration, transmission, and translation of molecular motions with greatest precision.(*28-30*) Because of the presence of the "Brownian storm" defined motions at molecular scales are very effectively equilibrated and randomized. Long range coupling and scaling up,(*31-36*) translation of one defined motion into another one,(*37-41*) or even power-stroke mechanisms(*42*) are therefore inherently difficult tasks at nanometer sizes. One important fundamental concept to translate small scale motions is molecular gearing(*7, 43-45*) in which intermeshed molecular fragments are moving in concert with each other. Different to the macroscopic world however, gearing processes are exceptionally hard to realize in the molecular world as friction and inertia do not play an important role here. As a consequence, slipping processes that evade true gearing are the rule rather than the exception even in highly intermeshed and sterically hindered molecular systems.(*7*) So far, mechanically controlled molecular systems have been developed ranging from more simple molecular breaks(*46, 47*) to truly geared systems in which different molecular fragments or entities move in concert because of their tight intermeshing (see ref. (*48-53*) for selected examples). More recent progress has allowed to switch gearing in an ON/OFF fashion.(*54*) Related molecular systems are able to control the speed of a particular sub-motion via switching processes.(*55, 56*) However, to the best of our knowledge functional gearing systems put forward so far are not powered directly by an energy source - although most recent efforts are moving in this direction.(*57, 58*) Instead, their motions are the result of thermal fluctuations and thus intrinsically passive and nondirectional.

In this work we present a novel concept enabling energy powered molecular gearing (Figure 1). Visible light is used as energy source actively fueling highly efficient gearing processes at the nanoscale within hemithioindigo(*59, 60*) (HTI)-gear **1**. We directly show that different to a thermal gearing process, photogearing can be by far the dominating motion within a molecular framework. At the same time translation of a 180° double bond isomerization into a 120° single bond rotation (SBR) is achieved by the employed bevel-gearing mechanism. Thus, a highly challenging precision-shift in the motion character (2-step to 3-step for a full 360° rotation) as well as spatial reorientation (120° angling) of the powered motion is demonstrated with our molecular system. We expect great prospects for the concept of photogearing, which allows to alleviate the problems of thermal gearing systems and enables direct powering of geared motions and the precise shifting of molecular motions. Such precision control at the smallest scales will be of great value to anyone interested in using ordered motions for governing

functions in chemical/nano systems. This approach will therefore strongly facilitate future research in many fields not least in integrated nanomachinery.

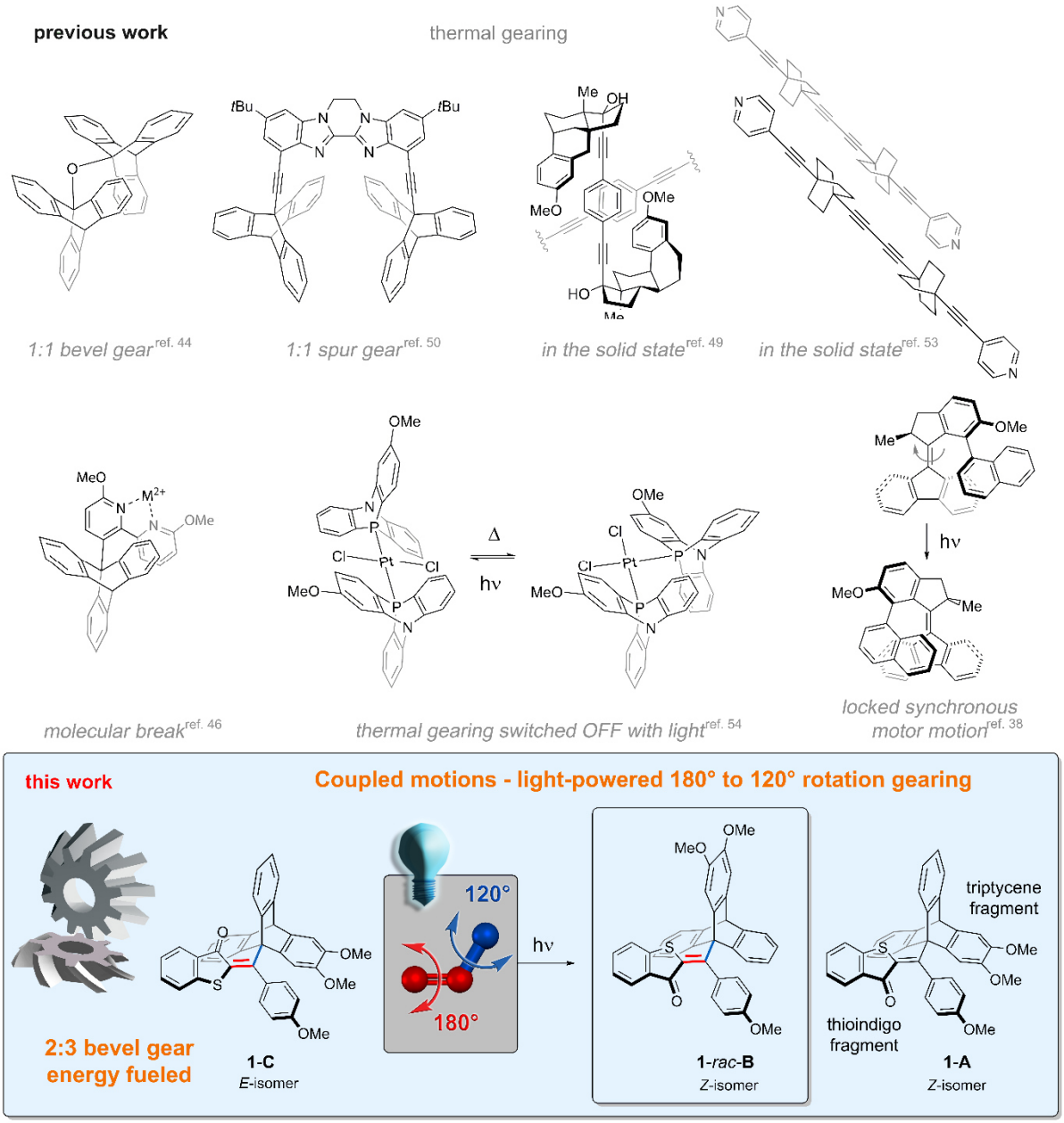

Figure 1 Thermal molecular gearing (top row), control of molecular rotation or gearing and related synchronous molecular motions (middle row) contrasted with the herein introduced photogearing as a distinct concept to directly power molecular gearing motions with light (bottom row).

Results and Discussion

Hemithioindigo (HTI)-based molecular gearing system **1** inherits a highly intermeshed nonsymmetric triptycene moiety, which is introduced as fourth substituent at the

photoisomerizable double bond (Figure 1 bottom row). Due to close proximity of the thioindigo and triptycene molecular fragments their effective intermeshing is achieved. The synthesis of this sterically strongly hindered system was accomplished using a recently reported method developed in our laboratory for the synthesis of sterically crowded HTI motors.(*61*) The synthesis proceeds in eight linear steps and is described in detail in the Supporting Information. HTI-gear **1** can adopt six distinct states. Three triptycene rotamers are accessible in both *Z* and *E* isomeric form, yet based on the symmetry of the triptycene fragment, two states present enantiomers and thus are not readily observed with classical spectroscopy methods, resulting in four distinct diastereomeric states. However, for the elucidation of different possible rotations and particularly the gearing processes it was not necessary to study individual enantiomers as both give rise to the same behavior. We label the four distinct isomers as depicted in Figure 2a with **A**, *rac*-**B**, **C**, and *rac*-**D**. Isomers **A** and *rac*-**B** inherit a *Z* configured isomerizable double bond and correspondingly isomers **C** and *rac*-**D** inherit an *E* configured double bond. Crystals suitable for X-ray analysis were obtained for isomers **A** and **C** facilitating direct assignment of solution spectral species (Figure 2a). A detailed analysis of solution NMR spectra allowed to further assign individual signals to the isomer structures (for details of solution conformation analysis see the Supporting Information).

As outlined in Figures 1, 2, and 3 the molecular setup of HTI-gear **1** allows to distinguish coupled gearing motions from sole uncoupled/slipping bond rotations as each process leads to interconversion between two different isomeric states. For example a gearing motion between the triptycene fragment and the thioindigo fragment can directly be observed as concomitant transition from isomer **A** to *rac*-**D** or isomer **C** to *rac*-**B** (example shown in Figure 1 bottom row) and *vice versa*. Sole single bond rotation (SBR) of the triptycene fragment on the other hand would result in interconversion between isomers **A** and *rac*-**B** or **C** and *rac*-**D** and sole double bond isomerization (DBI) would lead to interconversion between isomers **A** and **C** or *rac*-**B** and *rac*-**D**. Only conversion from isomer *rac*-**B** to *rac*-**D** and *vice versa* would be ambiguous as in this case a sole DBI and a gearing motion would lead to population of different respective enantiomers of **B** and **D**, which are not distinguished by conventional spectroscopy.

A first thermal analysis of the HTI-gear system **1** was conducted experimentally to elucidate its ground state energy profile and the corresponding thermally activated motions (Figure 2b to d). Pronounced heating of an *E* isomer enriched $C_2D_2Cl_4$-solution at 140 °C over a period of six hours produced an equilibrium mixture consisting of 64% of *Z* isomers (**A** and *rac*-**B**) and 36% of *E* isomers (**C** and *rac*-**D**). Using the *Gibbs-Helmholtz* equation an energy

difference of ΔG = 0.47 kcal·mol^{-1} between *Z* an *E* isomers could be obtained from the equilibrium distribution. A kinetic analysis of the conversion gives the corresponding *Gibbs* energy of activation $\Delta G^{\ddagger}$ = 32.4 kcal·mol^{-1} for thermal *E* to *Z* isomerization. Separated thermal isomer interconversion experiments for either *Z* or *E* configured rotamers were conducted at lower temperatures in CD_2Cl_2 solution. They revealed that isomer **A** is the thermodynamically most stable state overall. Additionally a highly selective conversion between exclusively isomers *rac*-**B** and **A** is taking place. When starting from a *rac*-**B** enriched solution thermal activation at 0 °C in the dark only leads to population of the **A** isomer evidencing sole single bond rotation around the triptycene-connecting single bond. A final ratio of **A** : *rac*-**B** = 62% : 38% was observed establishing an energy difference between *rac*-**B** and **A** of 0.44 kcal·mol^{-1}. Kinetic analysis of this thermal single bond rotation delivered a *Gibbs* energy of activation $\Delta G^{\ddagger}$ = 20.3 kcal·mol^{-1} for this motion. Similarly, the thermal behavior of the *E* configured isomers **C** and *rac*-**D** was scrutinized at 30 °C in CD_2Cl_2 solution. Again, thermal interconversion between only these two isomers is taking place and isomer *rac*-**D** was found to be 0.67 kcal/mol higher in energy compared to **C**. An associated *Gibbs* energy of activation $\Delta G^{\ddagger}$ = 22.2 kcal·mol^{-1}was determined for this thermal single bond rotation. Taking these data together, the whole ground state energy profile of HTI-gear **1** could experimentally be quantified. It was further found that exclusively slipping-motions – i.e. sole single bond rotations around the triptycene axis and no coupled gearing motions between the triptycene and thioindigo fragment are present under thermal activation.

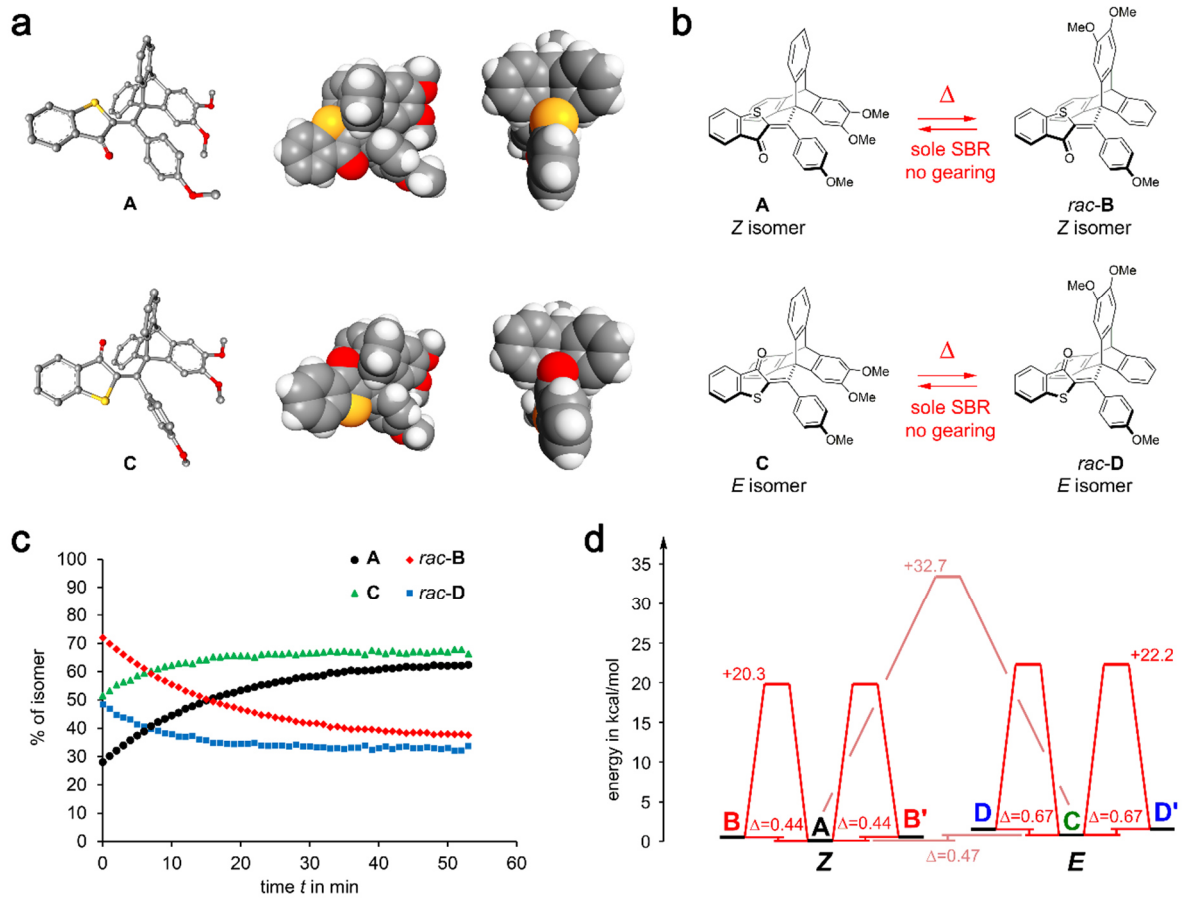

Figure 2 HTI-gear system **1** and its thermally activated motions. a) Structures of isomers **A** and **C** in the crystalline state. Space-filled depictions were chosen to illustrate the significant intermeshing of the thioindigo and triptycene fragments. b) Four different isomers are observable by conventional spectroscopy, **A** with *Z* configured central double bond, racemic isomer *rac*-**B** with *Z* configured double bond and the corresponding isomers **C** and *rac*-**D**, both with *E* configured double bonds. Only interconversions between rotamers **A** and *rac*-**B** as well as between **C** and *rac*-**D** are observed as thermally activated processes at ambient temperatures. SBR = single bond rotation. c) Kinetics of the selective thermal interconversion between rotamers **A** and *rac*-**B** at 0 °C and **C** and *rac*-**D** at 30 °C as measured by ^{1}H NMR spectroscopy. Kinetic analysis gives the corresponding *Gibbs* energies of activation. d) Experimentally established ground state energy profile for HTI-gear **1**.

The photochemistry of HTI-gear **1** was investigated next with the aid of Markov-Matrix kinetic analysis (Figure 3a) similar to a previously reported methodology.(*19, 62*) To this end it was necessary to use solutions significantly enriched in each isomer as the starting point of irradiation experiments. Selective isomer enrichment was possible either by crystallization to enrich isomers **A** and **C**, or by low temperature (–30 °C) HPLC separation and isolation of thermally labile isomers *rac*-**B** and *rac*-**D** prior to the actual irradiation experiments as outlined in detail in the Supporting Information. In this way we could establish four different starting

points for irradiations with either 95% **A**, 64% *rac*-**B**, 94% **C**, or 72% *rac*-**D** being present. Two additional isomeric mixtures were used to create two more different starting points (see Supporting Information). These different CD_2Cl_2 solutions were cooled to –40 °C to inhibit any thermally activated bond rotations within HTI-gear **1**, which could otherwise overshadow the pure photochemical behavior. Irradiation at –40 °C was conducted inside the NMR spectrometer with the aid of a fiber-coupled 420 nm LED and the progress of isomerization was followed by measuring ^{1}H NMR spectra in minute-time intervals (Figure 3b-e). In this way the photoconversion kinetics could be followed in detail over prolonged irradiation times without interference of thermal reactions. The relative propensities for isomer interconversions could be obtained directly from Markov analysis and simulation of the kinetic data (see Supporting Information for details). Very good agreement of simulated conversions and experimental data was obtained for this analysis, which unequivocally show significant photogearing for both *Z* and *E* isomeric **1**. For the *E* isomeric rotamers **C** and *rac*-**D** photogearing is in fact the dominating process. For example, isomer **C** undergoes photogearing with more than 2-fold higher propensity than the combined sole DBI of the thioindigo fragment and sole SBR of the triptycene moiety. This behavior is obvious even without Markov analysis as irradiation of the **C** enriched solution leads to a very steep increase of the *rac*-**B** isomer as compared to the much slower changes of all other isomers.

To obtain absolute values for the different photoconversion processes quantum yields were measured at –40 °C (Figure 3f and g). For this purpose a combination of photon counting and ^{1}H NMR spectroscopy was used to quantify the photoconversions between *Z* and *E* isomeric **1** (for details see the Supporting Information). When taking into account the relative photoconversion propensities as elucidated by Markov analysis, the quantum yields for all observable photoisomerization reactions within HTI-gear **1** could be obtained. For all photoconversion processes sizable quantum yields of up to 6.8% were obtained as shown in Figure 3a. As can be seen from the data, slipping motions are dominant in the *Z* configured isomers leading to pronounced sole DBI (ϕ(**A** to **C**) = 2%) and SBR (ϕ(**A** to *rac*-**B**) = 5.9% and ϕ(*rac*-**B** to *rac*-**D**) = 0.8%) in isomers **A** and *rac*-**B**. Nevertheless, a clear propensity for a photogearing motion is also observed in which both the central double bond and the adjacent single bond connecting to the triptycene fragment are rotated at the same time by 180° and 120°, respectively. This motion leads to conversion from **A** to *rac*-**D** or *rac*-**B** to **C** with sizable quantum yields of ϕ(**A** to *rac*-**D**) = 2% and ϕ(*rac*-**B** to **C**) = 0.4%. The ambiguous motion from *rac*-**B** to *rac*-**D** occurs with ϕ(*rac*-**B** to *rac*-**D**) = 2%.

In the *E* configured isomers **C** and *rac*-**D** photogearing is much more pronounced and the slipping motions are reduced significantly. For isomer **C**, DBI and SBR are decreased to ϕ(**C** to **A**) = 1.4% for the former and ϕ(**C** to *rac*-**D**) = 1.6% for the latter. For isomer *rac*-**D** the corresponding quantum yield for SBR is ϕ(*rac*-**D** to **C**) = 0.3%. The photogearing motion between central double bond and adjacent single bond connecting the triptycene fragment is most pronounced and dominant for isomer **C** proceeding with the highest overall quantum yield ϕ(**C** to *rac*-**B**) = 6.8%. The corresponding photogearing motion is also quite pronounced in the *rac*-**D** isomer with a quantum yield of ϕ(*rac*-**B** to *rac*-**D**) = 2.2%. For the *rac*-**D** isomer the ambiguous motion from *rac*-**D** to *rac*-**B** occurs with ϕ(*rac*-**D** to *rac*-**B**) = 3%.

Taking these numbers together a clear influence of the starting geometry on the effectiveness of photogearing can thus be discerned in HTI-gear system **1**. In the *E* isomeric forms photogearing represents a strongly favored process, as is directly observed for isomer **C**, for which all other possible photoconversion pathways are unambigously discernible. For the other *E* configured *rac*-**D** isomer photogearing is also observed as preferred photoconversion pathway. In this case the actual sum-quantum yield for photogearing could even be higher if suitable enantiomers of *rac*-**B** and *rac*-**D** are interconverting. This photogearing selectivity of the *E* isomers can in part be attributed to better intermeshing of the carbonyl group within the triptycene pocket. For the *Z* isomeric states the sulfur atom leads to inferior intermeshing between the thioindigo and triptycene fragments, which is directly observed by comparison of the molecular structures of **A** and **C** in the crystalline state (Figure 2a). However, electronic effects are likely to also play an important role as steric hindrance and intermeshing in HTI-gear **1** is clearly not enough to allow thermal gearing to take any effect. Therefore, a distinctly different behavior between ground state and excited state motions is observed, indicating a mechanistically different origin of the corresponding molecular rotations.

When comparing sum quantum yields it becomes apparent that both *Z* and *E* isomers behave similar and about 10% overall photoisomerization quantum yield is obtained for both **A** and **C**. Since the SBR photoreactions of isomers *rac*-**B** and *rac*-**D** are obscured their sum quantum yields are not known for comparison. It is interesting to note however, that the position of the triptycene moiety influences the propensity to undergo a specific photoreaction. Comparing isomer **C** with *rac*-**D** for example, photogearing proceeds with 6.8% quantum yield for the former, while for the latter only a maximum of 5.2% is possible (if ϕ(*rac*-**D** to *rac*-**B**) = 3.0% is fully allocated to photogearing). Additionally, SBR for the conversion from **C** to *rac*-**D** is significantly more effective (1.6%) than the reverse reaction (0.3%). Similarly, SBR from **A** to

rac-**C** is also much more efficient (5.9%) than the reverse reaction (0.8%). Again, electronic effects are expected to strongly affect these processes, since the triptycene blades are electronically distinct by their substitutions.

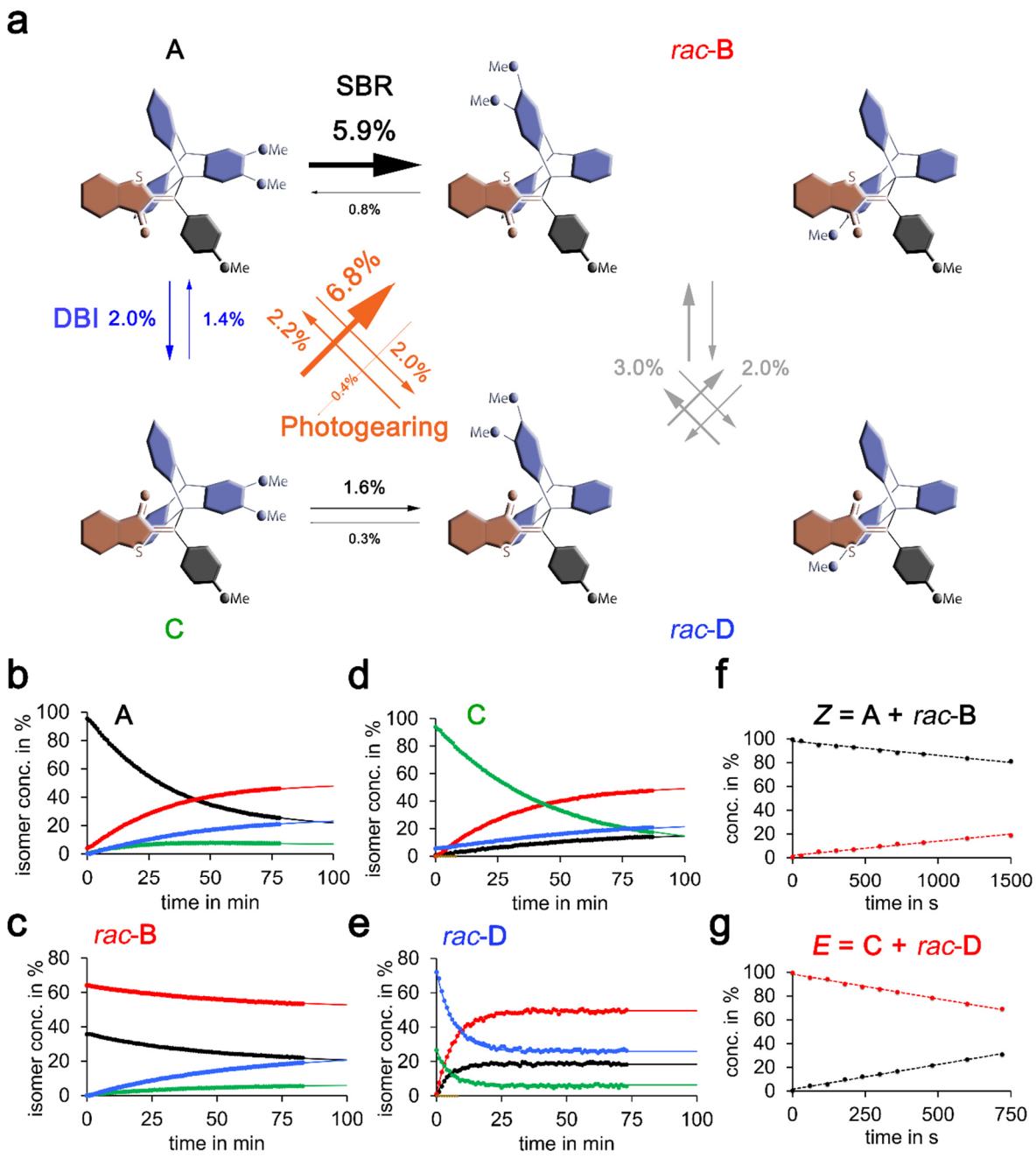

Figure 3 Photogearing in HTI-gear **1**. Photoconversions were measured by ^{1}H NMR (400 MHz) in CD_2Cl_2 at –40 °C by in-situ irradiation within the NMR spectrometer. Photoquantum yields for *Z* to *E* conversions and *vice versa* were measured by a combined method of photon-counting and ^{1}H NMR (400 MHz) spectroscopy in CD_2Cl_2. Afterwards the conversion propensities of individual isomers were scaled to the quantum yields measured for double bond photoisomerization (DBI). a) Measured

quantum yields for all photoconversions of individual isomers of HTI-gear **1**. Experimental (points) and simulated (lines) kinetics of the photoconversion of mainly isomer **A** (black circles, b); mainly isomer *rac*-**B** (red circles, c); mainly isomer **C** (green circles, d); and mainly isomer *rac*-**D**, (blue circles, e). f) Quantum yield measurements of *Z* (black circles) to *E* (red circles) photoisomerization by the initial slope method. g) Quantum yield measurements of *E* (red circles) to *Z* (black circles) photoisomerization by the initial slope method.

In summary, we have demonstrated a distinct and powerful concept - photogearing - for actively powering the precise translation of molecular motions. In our HTI-gearing system the 180° rotation of a planar thioindigo fragment is effectively translated to a 120° rotation of a nonsymmetric triptycene fragment. Therefore, a 2-to-3 translation of molecular motions is achieved by the correlated gearing process. At the same time the geared motions of the two molecular fragments are angled by about 120° similar to macroscopic bevel gear arrangements. The gearing motion is actively powered by the energy input of blue light irradiation and is shown to be dominating the light induced rotations of *E* configured isomers. The thermal behavior in contrast is distinctly different and only slipping motions i.e. uncorrelated motions between individual molecular fragments is observed. With photogearing it is thus possible to establish highly efficient and actively powered gearing motions at the nanoscale using light as external fuel. We thus are convinced that more sophisticated gearing systems can now be devised that translate precise molecular motions over longer distances, in different directions and with different speeds akin to integrated macroscopic gearing systems. Our study provides a distinct way for manipulating precise molecular motions and should open up a plethora of new possibilities and design concepts for the creation of future integrated nanomachinery.

Acknowledgements

H. Dube thanks the Deutsche Forschungsgemeinschaft (DFG) for an Emmy Noether fellowship (DU 1414/1-2). We further thank the Deutsche Forschungsgemeinschaft (SFB 749, A12) and the Cluster of Excellence “Center for Integrated Protein Science Munich” (CIPSM) for financial support.

References

1. J. P. Sauvage, From Chemical Topology to Molecular Machines (Nobel Lecture). *Angew. Chem. Int. Ed.* **56**, 11080-11093 (2017).
2. J. F. Stoddart, Mechanically Interlocked Molecules (MIMs)-Molecular Shuttles, Switches, and Machines (Nobel Lecture). *Angew. Chem. Int. Ed.* **56**, 11094-11125 (2017).
3. S. Erbas-Cakmak, D. A. Leigh, C. T. McTernan, A. L. Nussbaumer, Artificial Molecular Machines. *Chem. Rev.* **115**, 10081-10206 (2015).
4. E. R. Kay, D. A. Leigh, F. Zerbetto, Synthetic molecular motors and mechanical machines. *Angew. Chem. Int. Ed.* **46**, 72-191 (2007).
5. C. S. Vogelsberg, M. A. Garcia-Garibay, Crystalline molecular machines: function, phase order, dimensionality, and composition. *Chem. Soc. Rev.* **41**, 1892-1910 (2012).
6. J. D. Harris, M. J. Moran, I. Aprahamian, New molecular switch architectures. *Proc. Natl. Acad. Sci. U. S. A.* **115**, 9414-9422 (2018).
7. G. S. Kottas, L. I. Clarke, D. Horinek, J. Michl, Artificial Molecular Rotors. *Chem. Rev.* **105**, 1281-1376 (2005).
8. J. Michl, E. C. H. Sykes, Molecular Rotors and Motors: Recent Advances and Future Challenges. *ACS Nano* **3**, 1042-1048 (2009).
9. M. von Delius, E. M. Geertsema, D. A. Leigh, A synthetic small molecule that can walk down a track. *Nat. Chem.* **2**, 96-101 (2010).
10. M. J. Barrell, A. G. Campana, M. von Delius, E. M. Geertsema, D. A. Leigh, Light-driven transport of a molecular walker in either direction along a molecular track. *Angew. Chem. Int. Ed.* **50**, 285-290 (2011).
11. C. Cheng *et al.*, An artificial molecular pump. *Nat. Nanotechnol.* **10**, 547-553 (2015).
12. Y. Qiu *et al.*, A precise polyrotaxane synthesizer. *Science* **368**, 1247-1253 (2020).
13. N. Koumura, R. W. J. Zijlstra, R. A. van Delden, B. L. Feringa, Light-driven monodirectional molecular rotor. *Nature* **401**, 152-155 (1999).
14. J. V. Hernandez, E. R. Kay, D. A. Leigh, A Reversible Synthetic Rotary Molecular Motor. *Science* **306**, 1532-1537 (2004).
15. L. Greb, J. M. Lehn, Light-driven molecular motors: imines as four-step or two-step unidirectional rotors. *J. Am. Chem. Soc.* **136**, 13114-13117 (2014).
16. G. Haberhauer, A molecular four-stroke motor. *Angew. Chem. Int. Ed.* **50**, 6415-6418 (2011).
17. H. L. Tierney *et al.*, Experimental demonstration of a single-molecule electric motor. *Nat. Nanotechnol.* **6**, 625-629 (2011).
18. M. Guentner *et al.*, Sunlight-powered kHz rotation of a hemithioindigo-based molecular motor. *Nat. Commun.* **6**, 8406 (2015).
19. A. Gerwien, P. Mayer, H. Dube, Photon-Only Molecular Motor with Reverse Temperature-Dependent Efficiency. *J. Am. Chem. Soc.* **140**, 16442-16445 (2018).
20. A. Gerwien, P. Mayer, H. Dube, Green light powered molecular state motor enabling eight-shaped unidirectional rotation. *Nat. Commun.* **10**, 4449 (2019).
21. S. Kassem *et al.*, Artificial molecular motors. *Chem. Soc. Rev.* **46**, 2592-2621 (2017).
22. D. Roke, S. J. Wezenberg, B. L. Feringa, Molecular rotary motors: Unidirectional motion around double bonds. *Proc. Natl. Acad. Sci. U. S. A.* **115**, 9423-9431 (2018).

23. H. A. Kistemaker, P. Stacko, J. Visser, B. L. Feringa, Unidirectional rotary motion in achiral molecular motors. *Nat. Chem.* **7**, 890-896 (2015).
24. S. P. Fletcher, F. Dumur, M. M. Pollard, B. L. Feringa, A Reversible, Unidirectional Molecular Rotary Motor Driven by Chemical Energy. *Science* **310**, 80-82 (2005).
25. M. R. Wilson *et al.*, An autonomous chemically fuelled small-molecule motor. *Nature* **534**, 235-240 (2016).
26. S. Erbas-Cakmak *et al.*, Rotary and linear molecular motors driven by pulses of a chemical fuel. *Science* **358**, 340-343 (2017).
27. U. G. E. Perera *et al.*, Controlled clockwise and anticlockwise rotational switching of a molecular motor. *Nat. Nanotechnol.* **8**, 46-51 (2013).
28. I. Aprahamian, The Future of Molecular Machines. *ACS Cent. Sci.* **6**, 347-358 (2020).
29. T. van Leeuwen, A. S. Lubbe, P. Štacko, S. J. Wezenberg, B. L. Feringa, Dynamic control of function by light-driven molecular motors. *Nat. Rev. Chem.* **1**, (2017).
30. A. Goswami, S. Saha, P. K. Biswas, M. Schmittel, (Nano)mechanical Motion Triggered by Metal Coordination: from Functional Devices to Networked Multicomponent Catalytic Machinery. *Chem. Rev.* **120**, 125-199 (2020).
31. R. Eelkema *et al.*, Molecular machines: nanomotor rotates microscale objects. *Nature* **440**, 163 (2006).
32. J. Chen *et al.*, Artificial muscle-like function from hierarchical supramolecular assembly of photoresponsive molecular motors. *Nat. Chem.* **10**, 132-138 (2018).
33. J. Berna *et al.*, Macroscopic transport by synthetic molecular machines. *Nat. Mater.* **4**, 704-710 (2005).
34. J. Boelke, S. Hecht, Designing Molecular Photoswitches for Soft Materials Applications. *Adv. Optical Mater.* **7**, (2019).
35. Q. Li *et al.*, Macroscopic contraction of a gel induced by the integrated motion of light-driven molecular motors. *Nat. Nanotechnol.* **10**, 161-165 (2015).
36. D. Dattler *et al.*, Design of Collective Motions from Synthetic Molecular Switches, Rotors, and Motors. *Chem. Rev.* **120**, 310-433 (2020).
37. S. F. Pizzolato *et al.*, Central-to-Helical-to-Axial-to-Central Transfer of Chirality with a Photoresponsive Catalyst. *J. Am. Chem. Soc.* **140**, 17278-17289 (2018).
38. P. Štacko *et al.*, Locked synchronous rotor motion in a molecular motor. *Science* **356**, 964-968 (2017).
39. E. Uhl, S. Thumser, P. Mayer, H. Dube, Transmission of Unidirectional Molecular Motor Rotation to a Remote Biaryl Axis. *Angew. Chem. Int. Ed.* **57**, 11064-11068 (2018).
40. E. Uhl, P. Mayer, H. Dube, Active and Unidirectional Acceleration of Biaryl Rotation by a Molecular Motor. *ChemRxiv*, doi: 10.26434/chemrxiv.10048871.v10048871 (2019).
41. T. Muraoka, K. Kinbara, T. Aida, Mechanical twisting of a guest by a photoresponsive host. *Nature* **440**, 512-515 (2006).
42. R. D. Astumian, Trajectory and Cycle-Based Thermodynamics and Kinetics of Molecular Machines: The Importance of Microscopic Reversibility. *Acc. Chem. Res.* **51**, 2653-2661 (2018).
43. A. A. Gakh, R. A. Sachleben, J. C. Bryan, Molecular Gearing Systems. *Chemtech* **27**, 26-33 (1997).
44. H. Iwamura, K. Mislow, Stereochemical consequences of dynamic gearing. *Acc. Chem. Res.* **21**, 175-182 (1988).

45. I. Liepuoniute, M. J. Jellen, M. A. Garcia-Garibay, Correlated motion and mechanical gearing in amphidynamic crystalline molecular machines. *Chem. Sci.* **11**, 12994-13007 (2020).
46. T. R. Kelly *et al.*, A Molecular Brake. *J. Am. Chem. Soc.* **116**, 3657-3658 (1994).
47. J.-S. Yang *et al.*, A Pentiptycene-Derived Light-Driven Molecular Brake. *Org. Lett.* **10**, 2279-2282 (2008).
48. S. Perez-Estrada, B. Rodriguez-Molina, E. F. Maverick, S. I. Khan, M. A. Garcia-Garibay, Throwing in a Monkey Wrench to Test and Determine Geared Motion in the Dynamics of a Crystalline One-Dimensional (1D) Columnar Rotor Array. *J. Am. Chem. Soc.* **141**, 2413-2420 (2019).
49. B. Rodriguez-Molina *et al.*, Anisochronous dynamics in a crystalline array of steroidal molecular rotors: evidence of correlated motion within 1D helical domains. *J. Am. Chem. Soc.* **133**, 7280-7283 (2011).
50. D. K. Frantz, A. Linden, K. K. Baldridge, J. S. Siegel, Molecular spur gears comprising triptycene rotators and bibenzimidazole-based stators. *J. Am. Chem. Soc.* **134**, 1528-1535 (2012).
51. Y. Kawada, H. Iwamura, *J. Org. Chem.* **45**, 2547 (1980).
52. W. D. Hounshell, C. A. Johnson, A. Guenzi, F. Cozzi, K. Mislow, *Proc. Natl. Acad. Sci. USA* **77**, 6961 (1980).
53. C. Lemouchi *et al.*, Crystalline arrays of pairs of molecular rotors: correlated motion, rotational barriers, and space-inversion symmetry breaking due to conformational mutations. *J. Am. Chem. Soc.* **135**, 9366-9376 (2013).
54. H. Ube, Y. Yasuda, H. Sato, M. Shionoya, Metal-centred azaphosphatriptycene gear with a photo- and thermally driven mechanical switching function based on coordination isomerism. *Nat. Commun.* **8**, 14296 (2017).
55. A. S. Lubbe, N. Ruangsupapichat, G. Caroli, B. L. Feringa, Control of rotor function in light-driven molecular motors. *J. Org. Chem.* **76**, 8599-8610 (2011).
56. M. K. Ter Wiel, R. A. van Delden, A. Meetsma, B. L. Feringa, Control of rotor motion in a light-driven molecular motor: towards a molecular gearbox. *Org. Biomol. Chem.* **3**, 4071-4076 (2005).
57. S. Abid *et al.*, Desymmetrised pentaporphyrinic gears mounted on metallo-organic anchors. *Chem. Sci.* **12**, 4709-4721 (2021).
58. H. H. Lin, A. Croy, R. Gutierrez, C. Joachim, G. Cuniberti, Current-induced rotations of molecular gears. *J. Phys. Commun.* **3**, 025011 (2019).
59. S. Wiedbrauk, H. Dube, Hemithioindigo—an emerging photoswitch. *Tetrahedron Lett.* **56**, 4266-4274 (2015).
60. C. Petermayer, H. Dube, Indigoid Photoswitches: Visible Light Responsive Molecular Tools. *Acc. Chem. Res.* **51**, 1153-1163 (2018).
61. L. A. Huber *et al.*, Direct Observation of Hemithioindigo-Motor Unidirectionality. *Angew. Chem. Int. Ed.* **56**, 14536-14539 (2017).
62. A. Gerwien, M. Schildhauer, S. Thumser, P. Mayer, H. Dube, Direct evidence for hula twist and single-bond rotation photoproducts. *Nat. Commun.* **9**, 2510 (2018).